Available online at www.sciencedirect.com
ScienceDirect
Journal of Computational Physics 225 (2007) 615–634
JOURNAL OF COMPUTATIONAL PHYSICS
www.elsevier.com/locate/jcp

Direct numerical simulations of droplet emulsions in sliding bi-periodic frames using the level-set method

See Jo Kim [a], Wook Ryol Hwang [b,*]

[a] School of Mechanical Engineering, Andong National University, Songchun-dong 388, Andong, 760-749, Republic of Korea
[b] School of Mechanical and Aerospace Engineering, Research Center for Aircraft Parts Technology (ReCAPT), Gyeongsang National University, Gajwa-dong 900, Jinju 660-701, Republic of Korea

Received 6 August 2006; received in revised form 13 December 2006; accepted 20 December 2006
Available online 30 December 2006

Abstract

We present a direct numerical simulation technique for droplet emulsions of Newtonian–Newtonian system in simple shear flow. The Lees–Edwards type boundary condition has been incorporated with the sliding bi-periodic frame of Hwang et al. [W.R. Hwang, M.A. Hulsen, H.E.H. Meijer, Direct simulation of particle suspensions in sliding bi-periodic frames, J. Comput. Phys. 194 (2004) 742] for the continuous flow field problem and the level-set method with the continuous surface stress (CSS) formulation has been used for accurate description of the sharp interfaces. Based on the standard velocity–pressure formulation of the finite-element method, we use the mortar element method for the implementation of the sliding periodicity and employ the discontinuous Galerkin (DG) method for the stabilization of the interface advection equation. We present numerical results on the morphological development for a single, two and multiple drops in sliding bi-periodic frames for the demonstration of the feasibility of the present method in investigation of the relationship between the morphology and the bulk material responses such as the shear viscosity and the first normal stress difference.

Keywords: Direct numerical simulation; Emulsion; Lees–Edwards boundary condition; Sliding bi-periodic frame; Level set method; Continuous surface stress formulation; Finite element method; Bulk stress

1. Introduction

In this paper, we present a direct numerical simulation technique for Newtonian droplets suspended in a Newtonian fluid in simple shear flow, which usually involves complex morphological changes such as deformation, breakup and coalescence. The dynamics of the interface is determined by both the flow field that orients the interface and the interfacial tension which opposes this effect. Especially, we are interested in the inter-relationship between the morphological changes and the bulk material responses such as the shear viscosity and the first normal stress difference of this micro-structured material. Understanding this relationship is particularly important in the polymer industry, when blending two or more existing polymers. When two

* Corresponding author. Tel.: +82 55 751 6295; fax: +82 55 757 5622.
E-mail addresses: sjkim1@andong.ac.kr (S.J. Kim), wrhwang@gsnu.ac.kr (W.R. Hwang).

0021-9991/$ - see front matter © 2007 Elsevier Inc. All rights reserved.
doi:10.1016/j.jcp.2006.12.012

immiscible polymers are compounded in a mixing equipment, one often observes the formation of the dispersed two-phase mixture in which one component forms the discrete phase (drops) dispersed in the other component of the continuous phase (matrix). During the past decades numerous investigators have studied this system. The literature is reviewed, for example, by Han [1] and Tucker and Moldenaers [2]. However, the fundamental understanding of the droplet emulsion is still very limited. The main reason is that drops are deformable bodies and there are complicated many-body hydrodynamic interactions between them.

In order to deal with such a problem computationally, which is a many-deformable-body and time-dependent problem in nature, one needs a direct simulation technique that employs a well-defined periodic domain concept such that a single unit cell problem with a small number of droplets can represent the emulsion system containing a large number of droplets, eliminating the complicated drop-wall interaction. Moreover, the method should admit the usage of state-of-the-art viscoelastic constitutive equations in considering further extension to the polymeric blend which is of great importance in industry.

In 1972 Lees and Edwards [3] proposed a bi-periodic domain concept for Molecular Dynamics simulations by describing sliding boundary conditions for simple shear flow, which is nowadays called the Lees–Edwards boundary condition (LEbc). This scheme has been used with the Lattice Boltzmann method to solve the particle suspension [4], the phase separation [5] and the concentrated emulsion problems by a Lagrangian–Eulerian method with a re-meshing technique using Voronoi tessellation [6]. Recently, Hwang et al. [7] developed the sliding bi-periodic frame to extend the LEbc to the continuous field problems and combined it with the finite element method along with the fictitious-domain/mortar-element method to solve the particle suspension in the Eulerian fixed mesh. Furthermore, Hwang et al. [8] applied this scheme to the particle suspension formulated with a nonlinear viscoelastic fluid by incorporating the DEVSS/DG (Discrete Elastic Viscous Stress Splitting/Discontinuous Galerkin) method, which is one of the most robust formulation for the viscoelastic flow simulation currently available [10]. In addition, the sliding bi-periodic frame has been also adapted for the diffuse–interface method for simulations of droplet emulsion problems based on the stream function-vorticity formulation using the spectral element method (Anderson et al. [9]).

The numerical analyses on the drop deformation are numerous elsewhere: typically in Refs. [11–14] for the drop deformation by using the moving interface. For example, in our previous study [12,13], the finite element analysis for two-phase fluids was carried out in the entrance region of a cylindrical tube by a auto-remeshing technique. On the other hand, various numerical methods in a purely Eulerian framework have been developed that use a fixed mesh for the entire computation: e.g. the volume-of-fluid (VOF) method [15], the level-set method [16–18] and the diffuse–interface method [9,19]. In these methods, the interfacial tension can be treated either by the body force or by the surface stress, which are called the continuous surface force (CSF) model [20] and the continuous surface stress (CSS) model [21], respectively.

Our objective is the development of a direct numerical method to investigate the morphological developments in liquid–liquid emulsions and at the same time to investigate the relationship between the bulk material behaviors and the morphological information under simple shear flow. We employ the sliding bi-periodic frame of Hwang et al. [7] as a representative unit computational domain to treat the many-body problem in the droplet emulsion under simple shear flow. Also, to describe the sharp interface between the drop and the matrix fluid, we employ the level-set method, which is a popular and accurate method for the interface capturing, along with the CSS formulation.

The paper is organized as follows. First in Section 2 we define the problem and explain the basic governing equations. In Section 3 we explain the numerical methods and implementation techniques. Then in Section 4 we discuss expressions for the bulk stress in the sliding bi-periodic frame with the continuous surface stress formulation. In Section 5, we show results of three sets of example problems: simple shear flow with a single drop, two drops and multiple drops. Finally we end up with some conclusions.

2. Modeling

2.1. Problem definitions

In this paper, we consider a large number of deformable Newtonian droplets suspended in another Newtonian matrix fluid in simple shear flow. We restrict ourselves to two-dimensional systems and neglect inertia

for both fluids. Fig. 1 shows the sliding bi-periodic frames with a possible deformed drop configuration in a single frame. As time goes on, each frame translates at its own average velocity of the flow inside the frame and thereby rows of the frames slide relatively to one another by the amount Δ, which is determined by the given shear rate $\dot{\gamma}$, the elapsed time t, and the height of the frame H:

$$\Delta = \dot{\gamma} H t. \tag{1}$$

The sliding velocity of the frame is determined by the given shear rate and a representative vertical position of the frame based on an arbitrary global reference. Only the relative velocity inside the frame is important. In addition, the sliding frame is bi-periodic: the left and right boundaries satisfy the usual periodic condition and the upper and lower boundaries are subject to the time-dependent sliding periodicity described in Eq. (1). Therefore the motion of the drops as well as of the matrix fluid is subject to the time-dependent coupling between the upper and lower boundaries, in addition to the usual periodic condition in the horizontal direction [7].

As mentioned, a sliding bi-periodic frame, denoted by Ω, is the computational domain of this work (Fig. 1). The four boundaries of the domain are denoted by Γ_i $(i = 1, 2, 3, 4)$ and the symbol Γ will be used for $\bigcup_{i=1}^{4} \Gamma_i$. The Cartesian x and y coordinates are selected as parallel and normal to the shear flow direction, respectively. The regions occupied by the drops are denoted by $D_i(t)$ $(i = 1, \ldots, N)$ and N is the number of drops in a single frame at a certain time. We use a symbol $D(t)$ for $\bigcup_{i=1}^{N} D_i(t)$, a collective region occupied by drops at a certain time t. The boundary of the ith drop D_i is denoted by Φ_i and the symbol ϕ will be used for $\bigcup_{i=1}^{4} \Phi_i$. The vector $\boldsymbol{n}$ is the outward unit normal vector on the drop interface.

2.2. Governing equations

2.2.1. Equations for the matrix fluid and drops

The set of equations for the fluid domain is given by

$$\nabla \cdot \boldsymbol{\sigma}_{\mathrm{m}} = 0, \quad \text{in } \Omega \setminus D(t), \tag{2}$$

$$\nabla \cdot \boldsymbol{u}_{\mathrm{m}} = 0, \quad \text{in } \Omega \setminus D(t), \tag{3}$$

$$\boldsymbol{\sigma}_{\mathrm{m}} = -p_{\mathrm{m}} \boldsymbol{I} + 2\eta_{\mathrm{m}} \boldsymbol{D}_{\mathrm{m}}, \quad \text{in } \Omega \setminus D(t). \tag{4}$$

Eqs. (2)–(4) are equations for the momentum balance, the continuity and the constitutive relation, respectively. The subscript m denotes the matrix phase and $\boldsymbol{u}_{\mathrm{m}}$, $\boldsymbol{\sigma}_{\mathrm{m}}$, p_{m}, $\boldsymbol{I}$, $\boldsymbol{D}_{\mathrm{m}}$ and η_{m} are the velocity, the stress, the pressure, the identity tensor, the rate of deformation tensor and the viscosity, respectively, for the matrix phase. There is no explicit boundary condition on the domain boundary Γ. Instead we apply the sliding bi-periodic frame constraint on Γ later to assign simple shear flow condition, fulfilling the bi-periodicity of the computational domain.

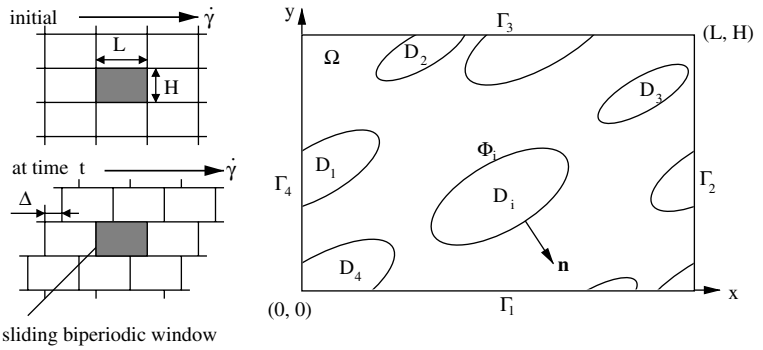

Fig. 1. Sliding bi-periodic frames in simple shear flow (left). A sliding bi-periodic frame is the computational domain of this work and a possible deformed drop configuration inside the domain is indicated (right).

The governing equations for a region occupied by a drop D_i at a certain time t can be written as:

$$\nabla \cdot \boldsymbol{\sigma}_{\mathrm{d}} = 0, \quad \text{in } D_i(t), \tag{5}$$

$$\nabla \cdot \boldsymbol{u}_{\mathrm{d}} = 0, \quad \text{in } D_i(t), \tag{6}$$

$$\boldsymbol{\sigma}_{\mathrm{d}} = -p_{\mathrm{d}}\boldsymbol{I} + 2\eta_{\mathrm{d}}\boldsymbol{D}_{\mathrm{d}}, \quad \text{in } D_i(t). \tag{7}$$

Note that the subscript d denotes the drop phase. Eqs. (5)–(7) are the equations for the momentum balance, the continuity and the constitutive relation, respectively, which are exactly the same as fluid domain equations in Eqs. (2)–(4) except for the drop viscosity η_{d}.

At the interface Φ between the drop and the suspending matrix, the following stress balance must be satisfied:

$$\boldsymbol{n} \cdot \boldsymbol{\sigma}_{\mathrm{m}} - \boldsymbol{n} \cdot \boldsymbol{\sigma}_{\mathrm{d}} = \zeta\kappa\boldsymbol{n}, \text{ on } \Phi, \tag{8}$$

where $\boldsymbol{n}$ is the local unit outward normal vectors to the interface and the variables ζ and κ denote the interfacial tension and the local mean curvature on the interface.

2.2.2. The level-set function

As mentioned in Section 1, there are several numerical approaches in handling the interface of the two-phase fluid system: the interface-tracking method, the volume-of-fluid method, the diffuse–interface method, the level-set method, etc. In the present work, the level-set method is employed for the description of the interface. The interface is not explicitly tracked but is defined to be the zero level set of a smooth function ϕ. The evolution equation for the level-set function ϕ can be expressed with the initial condition:

$$\frac{\partial \phi}{\partial t} + \boldsymbol{u} \cdot \nabla\phi = 0, \quad \phi|_{t=0} = \phi_0, \text{ in } \Omega. \tag{9}$$

The initial level-set function ϕ_0 is prescribed as the signed distance, which satisfies the following signed distance function property:

$$|\nabla\phi| = 1, \quad \text{and} \quad \phi|_{\Phi} = 0, \tag{10}$$

where ϕ is positive outside the drop and negative inside. When the function ϕ is seriously distorted as time evolves, it is necessary for the level-set function to restore the distance function property for the accurate solution of the evolution equation (Eq. (9)).

2.2.3. Governing equations with the CSS model

The governing equations for two separate phases can be expressed in a unified way for the entire domain, if the interfacial tension could be treated properly. Brackbill et al. [20] proposed the continuous surface force (CSF) model that considers the interfacial tension as a continuous body force acting on the interface. The body force, denoted by $\boldsymbol{f}_{\mathrm{s}}$, is given by:

$$\boldsymbol{f}_{\mathrm{s}} = -\zeta\kappa\boldsymbol{n}\delta(d), \tag{11}$$

where d and δ are the signed distance function and the Dirac delta function, respectively. In the continuous surface stress (CSS) model [21], the body force in Eq. (11) is replaced by the divergence of a stress tensor $\boldsymbol{\tau}_{\mathrm{s}}$, the continuous surface stress, as follows:

$$\boldsymbol{\tau}_{\mathrm{s}} = \zeta(\boldsymbol{I} - \boldsymbol{nn})\delta(d), \quad -\nabla \cdot \boldsymbol{\tau}_{\mathrm{s}} = \boldsymbol{f}_{\mathrm{s}}. \tag{12}$$

In this model, the interfacial tension is represented by the surface stress tensor $\boldsymbol{\tau}_{\mathrm{s}}$ that can be added in the constitutive equation as the additional stress:

$$\boldsymbol{\sigma} = -p\boldsymbol{I} + 2\eta\boldsymbol{D} + \boldsymbol{\tau}_{\mathrm{s}}, \quad \text{in } \Omega. \tag{13}$$

With this setting, the momentum balance and the continuity equation for the entire computational domain can be written simply by

$$\nabla \cdot \boldsymbol{\sigma} = 0, \quad \text{in } \Omega, \tag{14}$$

$$\nabla \cdot \boldsymbol{u} = 0, \quad \text{in } \Omega. \tag{15}$$

We note that the viscosity η in Eq. (13) can be taken with a jump across the interface, i.e., $\eta = \eta_m$ for $\phi > 0$, and $\eta = \eta_d$ for $\phi < 0$.

2.2.4. The sliding bi-periodic frame constraints

In the case of Newtonian flow simulation without considering drop deformation only two conditions need to be satisfied on the sliding bi-periodic frame boundary Γ: the continuity of the velocity field and the force balance. These conditions have been discussed in details in Hwang et al. [7]. However, in the present work with the level-set method, one needs an additional boundary condition, the inflow condition for the level-set function ϕ that is convected with the fluid velocity. Since the interface which crosses a boundary of the domain should re-appear on the corresponding periodic boundary, the inflow condition implies the continuity of ϕ between the periodic boundaries. The three conditions along the horizontal direction between Γ_2 and Γ_4 can be summarized as follows:

$$\boldsymbol{u}(0,y) = \boldsymbol{u}(L,y), \quad y \in [0,H], \tag{16}$$

$$\boldsymbol{t}(0,y) = -\boldsymbol{t}(L,y), \quad y \in [0,H], \tag{17}$$

$$\phi(0,y) = \phi(L,y), \quad y \in [0,H], \tag{18}$$

where the vector $\boldsymbol{t}$ denoting the traction force on the boundary.

The conditions for the sliding periodicity in the vertical direction are more complicated because of the time-dependent coupling between Γ_1 and Γ_3 as in Eq. (1). Below are the condition for the velocity continuity, the force balance and the continuity of the level-set function, respectively:

$$\boldsymbol{u}(x,H;t) = \boldsymbol{u}(\{x - \dot{\gamma}Ht\}^*,0;t) + \boldsymbol{f}, \quad x \in [0,L), \tag{19}$$

$$\boldsymbol{t}(x,H;t) = -\boldsymbol{t}(\{x - \dot{\gamma}Ht\}^*,0;t), \quad x \in [0,L), \tag{20}$$

$$\phi(x,H;t) = \phi(\{x - \dot{\gamma}Ht\}^*,0;t), \quad x \in [0,L), \tag{21}$$

where $\boldsymbol{f} = (\dot{\gamma}H, 0)$ and $\{\cdot\}^*$ denotes the modular function of L. (For example, $\{1.7L\}^* = 0.7L$ and $\{-1.7L\}^* = 0.3L$.)

In the weak formulation, the kinematic constraints (Eqs. (16) and (19)), called the sliding bi-periodic frame constraints, are usually combined with Lagrangian multipliers and then the associated force balances (Eqs. (17) and (20)) are satisfied implicitly through the multipliers. The continuity conditions for ϕ (Eqs. (18) and (21)) will be treated separately through the jump convection term in the discontinuous Galerkin (DG) formulation, which will be discussed in Section 3.1.

3. Numerical methods

We derived the weak form for the particle suspensions with the sliding bi-periodic frame constraint in the previous work [7]. Now we extend our previous formulation to incorporate the interfacial tension in the droplet emulsion problem. We use the discontinuous Galerkin (DG) method of Fortin and Fortin [22] for the stabilization of the convection equation of the level-set function (Eq. (9)).

3.1. Weak form

As we did in our previous work [7], we introduce two different Lagrangian multipliers, $\boldsymbol{\lambda}^h$ and $\boldsymbol{\lambda}^v$, which are associated with the kinematic constraint equation for the periodicity in the horizontal direction (Eq. (16)) and that for the sliding periodicity in the vertical direction (Eq. (19)):

$$\boldsymbol{\lambda}^h = \left(\lambda_x^h, \lambda_y^h\right) \in L^2(\Gamma_4)^2, \quad \boldsymbol{\lambda}^v = \left(\lambda_x^v, \lambda_y^v\right) \in L^2(\Gamma_3)^2.$$

Introducing the separate functional spaces U, P and ϕ for $\boldsymbol{u}$, p and ϕ, respectively, over the whole domain including the interior of the drop, the weak form for the entire domain can be constructed, along with the DG formulation for the evolution equation of the level-set function:

For $t > 0$, find $\boldsymbol{u} \in \mathsf{U}$, $p \in \mathsf{P}$, $\phi \in \Phi$, $\boldsymbol{\lambda}^{\mathrm{h}} \in L^2(\Gamma_4)^2$, $\boldsymbol{\lambda}^{\mathrm{v}} \in L^2(\Gamma_3)^2$ such that

$$-\int_\Omega p\nabla\cdot\boldsymbol{v}\mathrm{d}A + \int_\Omega 2\eta\boldsymbol{D}[\boldsymbol{u}]:\boldsymbol{D}[\boldsymbol{v}]\mathrm{d}A + \left(\boldsymbol{\lambda}^{\mathrm{h}}, \boldsymbol{v}(0,y)-\boldsymbol{v}(L,y)\right)_{\Gamma_4} + \left(\boldsymbol{\lambda}^{\mathrm{v}}, \boldsymbol{v}(x,H;t)-\boldsymbol{v}(\{x-\dot{\gamma}Ht\}^*,0;t)\right)_{\Gamma_3}$$
$$= -\int_\Omega \boldsymbol{\tau}_s:\boldsymbol{D}[\boldsymbol{v}]\mathrm{d}A, \tag{22}$$

$$\int_\Omega q\nabla\cdot\boldsymbol{u}\mathrm{d}A = 0, \tag{23}$$

$$\int_\Omega \psi\left(\frac{\partial\phi}{\partial t}+\boldsymbol{u}\cdot\nabla\phi\right)\mathrm{d}A - \sum_e\int_{\Gamma_e^{\mathrm{in}}}\psi(\phi-\phi^{\mathrm{ext}})(\boldsymbol{u}\cdot\boldsymbol{n}_e)\mathrm{d}s = 0, \tag{24}$$

$$(\boldsymbol{\mu}^{\mathrm{h}}, \boldsymbol{u}(0,y)-\boldsymbol{u}(L,y))_{\Gamma_4} = 0, \tag{25}$$

$$(\boldsymbol{\mu}^{\mathrm{v}}, \boldsymbol{u}(x,H;t)-\boldsymbol{u}(\{x-\dot{\gamma}Ht\}^*,0;t))_{\Gamma_3} = (\boldsymbol{\mu}^{\mathrm{v}},\boldsymbol{f})_{\Gamma_3}, \quad \boldsymbol{f}=(\dot{\gamma}H,0), \tag{26}$$

$$\phi|_{t=0} = \phi_0, \quad \text{in } \Omega. \tag{27}$$

for all $\boldsymbol{v} \in \mathsf{U}$, $q \in \mathsf{P}$, $\psi \in \Phi$, $\boldsymbol{\mu}^{\mathrm{h}} \in L^2(\Gamma_4)^2$, $\boldsymbol{\mu}^{\mathrm{v}} \in L^2(\Gamma_3)^2$. In Eq. (24), $\boldsymbol{n}_e$ is the unit outward normal vector on the boundary of an element e, Γ_e^{in} is the part of the boundary of element e where $\boldsymbol{u}\cdot\boldsymbol{n}_e < 0$ and ϕ^{ext} is the level-set function in the neighboring upwind element. The inner product $(\cdot,\cdot)_{\Gamma_j}$ is the standard inner product in $L^2(\Gamma_j)$:

$$(\boldsymbol{\mu},\boldsymbol{v})_{\Gamma_j} = \int_{\Gamma_j}\boldsymbol{\mu}\cdot\boldsymbol{v}\mathrm{d}s.$$

We have several remarks on the weak form in Eqs. (22)–(27).

(1) The level-set function ϕ from Eq. (24) will be used to determine the signed distance function $\mathrm{d}(\boldsymbol{x})$ in Eq. (12) by a direct geometrical re-distancing method. The re-distancing technique will be explained in Section 3.2.
(2) The inflow condition of the level-set function (Eqs. (18) and (21)) on the domain boundary has been incorporated with the DG formulation (Eq. (24)), by taking the external value ϕ^{ext} from the coupled position of the corresponding periodic boundary.
(3) Introducing a higher order interpolation of ϕ, one can simply increase the accuracy in determining the location of the interface with the subdivision of the element and the distance function d avoiding a large number of coupled equations, since the DG method uses discontinuous interpolation within the element level. (The sub-division of the element will be discussed later in Section 3.2.)
(4) To obtain simple shear flow in the x direction with the upper sliding boundary velocity of $\frac{1}{2}\dot{\gamma}H$ and that of the lower one of $-\frac{1}{2}\dot{\gamma}H$, we assign a zero velocity at the center of Γ_4 for all problems in this work [7].
(5) The pressure level of the fluid domain is determined by specifying one of the normal component of the Lagrangian multipliers on $\Gamma(\lambda_x^{\mathrm{h}}$ or $\lambda_y^{\mathrm{v}})$, since the multiplier can be identified as the traction force [7].

3.2. Interface capturing

As the level-set function evolves in time, the distance function property of Eq. (10) is no longer satisfied. In this case the level-set function has to be re-initialized to restore the property of the signed distance function, usually by solving a proper partial differential equation. The accuracy of the signed distance function is crucial for the evaluation of the interfacial stress $\boldsymbol{\tau}_{\mathrm{s}}$. In this work, we obtain the signed distance function by a direct geometrical re-distancing method as explained below.

The level-set function is the solution of the convection equation (Eq. (9)). Once the level-set function is set, one can find a finite number of discrete line segments along the interface with the level-set function being zero. We use a one-dimensional search on the element boundary (or sub-element boundary which will be discussed later). Then the distance function for a node in the computational domain is determined by the shortest distance from the node to the line segments. The sign of the distance function is assigned the same as that of the level-set function. In this manner, the new distance function can be obtained and we call this the direct geometrical re-distancing scheme [23]. For a given domain discretization, the accuracy of the distance function

highly depends on the accuracy of the line segments for the interface description and the accuracy of the line segments is determined by the accuracy of the level-set function. The DG method in solving the evolution equation of the level-set function is particularly preferred, since one can easily introduce a higher-order interpolation for the level-set function without increasing the computational cost seriously due to the minimal coupling between elements of the DG method.

We use the discontinuous bi-quadratic interpolation for the level-set function in this study. At least the second-order accuracy of the level-set function is necessary, in that the number of line segments can be increased to obtain the better description of the interface simply by changing the degree of sub-division in the element. (In case of the linear interpolation of the level-set function, the subdivision of an element hardly improves the accuracy of the distance function.) The line segments are searched along boundaries of the sub-divided element as shown in Fig. 2. We tested several degrees of subdivision from 1×1 to 8×8 for an element. We discuss the effect of the subdivision on the solution accuracy in Section 5.1. It would be worthwhile to mention a possible extension of this direct geometrical re-distancing scheme for 3D problems. In 3D, one has to discrete surface segments composed of triangular elements. Once the level-set function is set in an element (or sub-element), a finite number of discrete triangular meshes on the interface surface with the level-set function being zero in the element. The distance function for a given node is determined by the shortest distance from the node to the discrete surface elements.

Once the distance function is set, we evaluate the interfacial stress $\boldsymbol{\tau}_s$ using Eq. (12). The delta function δ and the unit normal vector $\boldsymbol{n}$ in Eq. (12) can be evaluated in terms of the signed distance function. To describe the delta function numerically, we introduce a smooth continuous function:

$$\delta(d)=\begin{cases}\frac{1}{2\varepsilon}+\frac{1}{2\varepsilon}\cos\left(\frac{\pi d}{\varepsilon}\right) & \text{for } -\varepsilon\leqslant d\leqslant\varepsilon,\\ 0, & \text{otherwise,}\end{cases} \tag{28}$$

where ε is chosen $1.5h$ with h being the mesh size. We note that the normal vector $\boldsymbol{n}$ is the gradient of the signed distance function whose magnitude is always equal to one. That is, the interfacial stress $\boldsymbol{\tau}_s$ can be evaluated as

$$\boldsymbol{\tau}_s=\zeta(\boldsymbol{I}-\nabla d\nabla d)\delta(d). \tag{29}$$

The evolution of the level-set function is performed separately from the signed distance function and the signed distance function is used mainly to evaluate the interfacial stress $\boldsymbol{\tau}_s$ (Eq. (29)). However, we re-initialize the level-set function using the signed distance function at a certain strain unit to avoid seriously distorted level-set function distribution. In this way, we can apply a higher-order time-stepping method such as the second-order Adams–Bashforth (AB2) or TVD-RK3 (Total-Variation-Diminishing/3rd-order Runge–Kutta) [24] in solving the evolution equation of the level-set function.

We remark that the distribution of the initial level-set function ϕ_0, satisfying the signed distance function property, should fulfill the bi-periodicity of the sliding bi-periodic frame. The care should be exercised in imposing ϕ_0 for an initial configuration with many and split droplets. Also, since the drop can be split into more than two parts possibly located in the opposite side of the boundary and the drop in the opposite side might be closest to a node, it is necessary to find the actual distance from a node to the object in the sliding bi-periodic frame context. To do so, we tried all the possible relocations of line segments according to the

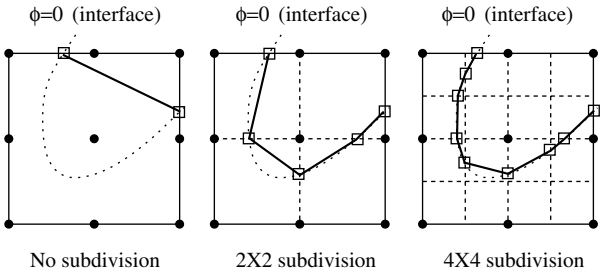

Fig. 2. The interface capturing method by subdivision of the element. The dotted line indicates the interface and the thick bold line indicates the line segment that is used to determine the distance function distribution.

time-dependent periodicity in the sliding bi-periodic frame, when measuring the distance. In addition, in evaluating $\boldsymbol{\tau}_s$ at a node (Eq. (29)) using $\nabla d\,(=\boldsymbol{n})$, one has to take the average of the ∇d values from the surrounding elements for the node. For the node on the boundary, one has to consider also the corresponding element on the opposite side (generally non-conforming) in the sliding bi-periodic frame. As an alternative way to circumvent this problem, we introduce a bit extended computation domain (by the amount of 2ε on each boundary). We copy the distance function data in the opposite side to the corresponding location near the node, by introducing the additional elements outside the boundary. The additional elements (conforming with the element on the boundary) together with the elements in the original domain constitute a bit extended domain. Considering the thickness of the smeared-out numerical delta function $\delta(d)$ of 2ε, the thickness of the additional element has been chosen as 2ε.

3.3. Implementation

3.3.1. Spatial discretization

For the discretization of the weak form, we use the regular quadrilateral element with the continuous bi-quadratic interpolation (Q_2) for the velocity $\boldsymbol{u}$, the discontinuous linear interpolation (P_1) for the pressure p and the discontinuous bi-quadratic interpolation (Q_2^d) for the level-set function ϕ. The boundary integrals Eqs. (22) and (25) for the horizontal periodicity have been discretized by using the point collocation method for all nodes (nodal collocation), since the facing elements between Γ_2 and Γ_4 are conforming. For the vertical sliding periodicity between non-conforming elements on Γ_1 and Γ_4, we use the mortar element technique with the continuous linear interpolation of $\boldsymbol{\lambda}^{\mathrm{v}}$ which has been verified to guarantee the optimal convergence of the kinematic compatibility and the force balance [7].

3.3.2. Time integration

At $t = 0$ the level-set function is set to be the initial signed distance function over the entire computational domain (Eq. (27)). We solve the momentum equation with the constraint equations (Eqs. (22), (23), (25), (26)) to get the velocity distribution at the initial time step. (See Step 4 with Eq. (32) below.) Then, at each time step, the following procedures are conducted.

Step 1 Get the level-set function ϕ^{n+1} by integrating the evolution equation of the level-set function (Eq. (24)) using $\boldsymbol{u}^n$ (the explicit third-order accurate TVD-RK3 scheme [24] combined with discontinuous Galerkin method: DG/TVD-RK3)

$$
\begin{aligned}
&[M]\left(\frac{\phi^{n+1}-\phi^{n}}{\Delta t}\right) = \boldsymbol{g}(\boldsymbol{u}^n,\phi^n)\\
&[M]\left(\frac{\phi^{n+2}-\phi^{n+1}}{\Delta t}\right) = \boldsymbol{g}\big(\boldsymbol{u}^n,\phi^{n+1}\big), \quad \phi^{n+0.5} = \frac{1}{4}\big(3\phi^n+\phi^{n+2}\big)\\
&[M]\left(\frac{\phi^{n+1.5}-\phi^{n+0.5}}{\Delta t}\right) = \boldsymbol{g}\big(\boldsymbol{u}^n,\phi^{n+0.5}\big)\\
&\phi^{n+1} = \frac{1}{3}\big(\phi^n+2\phi^{n+1.5}\big),
\end{aligned}
\tag{30}
$$

where $[M]$ is the mass matrix and the vector $\boldsymbol{g}$ is the forcing term which appears in the evolution equation of ϕ (Eq. (24)).

Step 2 Set the distance function d^{n+1} from the level-set function ϕ^{n+1} by the direct geometrical re-distancing scheme described in Section 3.2.

Step 3 Evaluate the interfacial stress tensor $\boldsymbol{\tau}_s^{n+1}$, from the given distribution of the distance function d^{n+1}:

$$
\boldsymbol{\tau}_s^{n+1} = \zeta(\boldsymbol{I}-\nabla d^{n+1}\nabla d^{n+1})\delta(d^{n+1}). \tag{31}
$$

Step 4 Get the remaining solutions $(\boldsymbol{u}^{n+1}, p^{n+1}, \boldsymbol{\lambda}^{\mathrm{h},n+1}, \boldsymbol{\lambda}^{\mathrm{v},n+1})$ by solving Eqs. (22), (23), (25), (26) implicitly using $\boldsymbol{\tau}_s^{n+1}$:

$$-\int_\Omega p^{n+1}\nabla\cdot\boldsymbol{v}\mathrm{d}A+\int_\Omega 2\eta\boldsymbol{D}[\boldsymbol{u}^{n+1}]:\boldsymbol{D}[\boldsymbol{v}]\mathrm{d}A+(\boldsymbol{\lambda}^{\mathrm{h},n+1},\boldsymbol{v}(0,y)-\boldsymbol{v}(L,y))_{\Gamma_4}$$
$$+(\boldsymbol{\lambda}^{v,n+1},\boldsymbol{v}(x,H)-\boldsymbol{v}(\{x-\dot\gamma Ht^{n+1}\}^*,0))_{\Gamma_3}=-\int_\Omega\boldsymbol{\tau}_{\mathrm{s}}^{n+1}:\boldsymbol{D}[\boldsymbol{v}]\mathrm{d}A, \tag{32a}$$

$$\int_\Omega q\nabla\cdot\boldsymbol{u}^{n+1}\mathrm{d}A=0, \tag{32b}$$

$$(\boldsymbol{\mu}^{\mathrm{h}},\boldsymbol{u}^{n+1}(0,y)-\boldsymbol{u}^{n+1}(L,y))_{\Gamma_4}=0, \tag{32c}$$

$$(\boldsymbol{\mu}^{\mathrm{v}},\boldsymbol{u}^{n+1}(x,H)-\boldsymbol{u}^{n+1}(\{x-\dot\gamma Ht^{n+1}\}^*,0))_{\Gamma_3}=(\boldsymbol{\mu}^{v},\boldsymbol{f})_{\Gamma_3}. \tag{32d}$$

In the Step 1, Eq. (30) can be solved at the element level, leading to a minimal coupling between elements. In the Step 4, one needs to solve a large sparse matrix equation with many zeroes on the diagonal which has been solved by a direct method based on a sparse multifrontal variant of Gaussian elimination (HSL/MA41) [25–27].

4. Bulk stress

The bulk stress is the average stress over the domain and, for Newtonian droplet emulsions in the absence of inertia, it can be written as:

$$\langle\boldsymbol{\sigma}\rangle=-P\boldsymbol{I}+2\eta_{\mathrm{m}}\langle\boldsymbol{D}\rangle-\frac{\eta_{\mathrm{m}}-\eta_{\mathrm{d}}}{V}\int_\Phi(\boldsymbol{un}+\boldsymbol{nu})\mathrm{d}S-\frac{\zeta}{V}\int_\Phi\left(\boldsymbol{nn}-\frac{1}{3}\boldsymbol{I}\right)\mathrm{d}S, \tag{33}$$

where P is the isotropic pressure and $\langle\cdot\rangle$ denotes the volume average quantity in the domain V [28]. In Eq. (33), the third term is the stress contribution of the drop phase due to the difference in the viscosity and the last term is the contribution from the interfacial tension ζ. These two are considered to be the component contribution [28]. As one expects from Eq. (33), it is crucial to accurately know not only the velocity field but also the configuration (shape and orientation) of the interface for the correct evaluation of the component contribution However, the accuracy of the interface configuration is limited in nature for the numerical methods based on the purely Eulerian framework such as the level-set method, when one attempts to compute the bulk stress directly from Eq. (33). The main reason is the accuracy in evaluation of the outward normal vector $\boldsymbol{n}$ on interface that requires the spatial derivatives of the level-set function or of the signed distance function, which inevitably involves an additional approximation.

In this work, we use an alternative expression of the bulk stress that does not require the evaluation of the normal vector $\boldsymbol{n}$ on the interface, by using the Lagrangian multipliers for the sliding bi-periodic frame constraints. The expression is quite similar to that for the particle suspension in sliding bi-periodic frame in Hwang et al. [7]. First, we note that the bulk stress can be evaluated by the integral of the traction force along the boundary only. That is,

$$\langle\boldsymbol{\sigma}\rangle=\frac{1}{V}\int_{\partial V}\boldsymbol{xt}\mathrm{d}S\left(=\frac{1}{A}\int_{\partial\Gamma}\boldsymbol{xt}\mathrm{d}s\right), \tag{34}$$

where $\boldsymbol{t}$ is traction force acting on the domain boundary ∂V and the expression in the parenthesis is for the sliding bi-periodic frame of area A. Then, we express the traction force using the Lagrangian multipliers, $\boldsymbol{\lambda}^{\mathrm{h}}$ and $\boldsymbol{\lambda}^{\mathrm{v}}$, that has been derived in Hwang et al. [7], from the comparison of the standard weak form with the prescribed traction and the augmented weak form of the momentum balance (Eq. (22)). Finally, one can obtain the bulk stress expression by the boundary integral of the Lagrangian multipliers that avoids using the normal vector $\boldsymbol{n}$ on the interface as follows:

$$\langle\sigma_{11}\rangle=\frac{1}{A}\int_0^L(\{x-\dot\gamma Ht\}^*-x)\lambda_x^v(x)\mathrm{d}x+\frac{1}{H}\int_0^H\lambda_x^h(y)\mathrm{d}y, \tag{35a}$$

$$\langle\sigma_{22}\rangle=-\frac{1}{L}\int_0^L\lambda_y^v(x)\mathrm{d}x, \tag{35b}$$

$$\langle\sigma_{12}\rangle=\frac{1}{A}\int_0^L(\{x-\dot\gamma Ht\}^*-x)\lambda_y^v(x)\mathrm{d}x+\frac{1}{H}\int_0^H\lambda_y^h(y)\mathrm{d}y$$
$$=-\frac{1}{L}\int_0^L\lambda_x^v(x)\mathrm{d}x. \tag{35c}$$

We remark that the bulk stress can be evaluated accurately also by the direct domain integral without considering the interface configuration, when using the CSS formulation for the equi-viscosity case ($\eta^{\mathrm{m}} = \eta^{\mathrm{d}} = \eta$). The stress at a point can be expressed as the constitutive equation of the CSS model: $\boldsymbol{\sigma} = -p\boldsymbol{I} + 2\eta\boldsymbol{D} + \boldsymbol{\tau}_{\mathrm{s}}$. Note that the interfacial stress $\boldsymbol{\tau}_{\mathrm{s}}$ is the distributed stress, though narrow, in the vicinity of the interface and is zero elsewhere. Therefore, one can directly integrate the above constitutive equation over the domain to evaluate the bulk stress. By comparison with Eq. (33), one get the following identity:

$$\langle \boldsymbol{\tau}_{\mathrm{s}} \rangle = \frac{1}{V}\int_V \boldsymbol{\tau}_{\mathrm{s}} \mathrm{d}V = -\frac{\zeta}{V}\int_\Phi \left(\boldsymbol{nn} - \frac{1}{3}\boldsymbol{I}\right)\mathrm{d}S. \tag{36}$$

This means that one can evaluate the interfacial contribution to the bulk stress by the direct domain integral without considering the interface configuration, since it is already included in the interfacial stress $\boldsymbol{\tau}_{\mathrm{s}}$. In the present paper, we evaluate the bulk stress using Eqs. (35) and, for the purpose for verification, the domain integral results will be compared with those from the boundary integrals for equi-viscosity system.

5. Example problems

5.1. A single drop problem

In the first example problem, we verify our formulation and implementation techniques using a single drop problem. The initial drop shape is circular and the radius R is 0.2. The dimension of the sliding bi-periodic frame is $(L, H) = (1, 1)$. The shear rate $\dot{\gamma}$ and the interfacial tension ζ are 1 and 0.4, respectively. The matrix and drop viscosity are the same ($\eta^{\mathrm{m}} = \eta^{\mathrm{d}} = 1$). The capillary number, an important parameter on the drop deformation, is defined as the viscous force over the capillary force:

$$Ca = \eta_{\mathrm{m}}\dot{\gamma}R/\zeta,$$

where R is the undeformed radius of the drop. Therefore the capillary number is 0.5 in the test problem. When presenting the bulk stress results, we use the shear viscosity $\bar{\eta}$ and the first normal stress difference $\overline{N}_1$ which are defined as

$$\bar{\eta} = \frac{\langle \sigma_{12} \rangle}{\eta_{\mathrm{m}}\dot{\gamma}} \quad \text{and} \quad \overline{N}_1 = \langle \sigma_{11} - \sigma_{22} \rangle.$$

The first normal stress difference is related with the anisotropy in the morphology of the droplet emulsion. Unless otherwise stated, the bulk stress is computed by the boundary integral of the Lagrangian multipliers (Eqs. (35)) throughout this work. Also, the re-initialization of the level-set function by the distance function has been performed every 0.5 strain unit for all the works presented here.

5.1.1. Convergence test

The first verification problem is the mesh refinement test. We locate initially the single drop at the center of the computational domain $(0.5, 0.5)$. We use three different finite element meshes: 10×10 (denoted by $h = 1/10$), 20×20 ($h = 1/20$) and 40×40 ($h = 1/40$) and the corresponding time steps Δt are 0.02, 0.01 and 0.005, respectively. In this test, we use the 4×4 sub-division of the element in searching the line segments along the interface. Results are presented in Fig. 3 and in Table 1 for the drop shape at $t = 4.8$, the shear viscosity and the first normal stress difference. All three results show good convergence with the mesh refinement. Only the very coarse mesh of $h = 1/10$ shows the discrepancy in the shear viscosity and the deformed drop shape. This implies that four elements inside the drop near the circular shape is not enough for a proper description of its deformation. The dependence of the first normal stress difference on the deformed drop shape is found to be minor in this case.

5.1.2. The sub-division of the element

Secondly, we investigate the effect of degree of sub-division of the element in searching the line segments along the interface. Again, we locate the single drop at the domain center and we use a $h = 1/20$ mesh with $\Delta t = 0.01$. Four different degrees of subdivision have been tested: 1×1 (no sub-division), 2×2, 4×4 and 8×8. Plotted in Fig. 4 and listed in Table 2 are again the drop shape at $t = 4.8$, the shear viscosity and the first normal stress

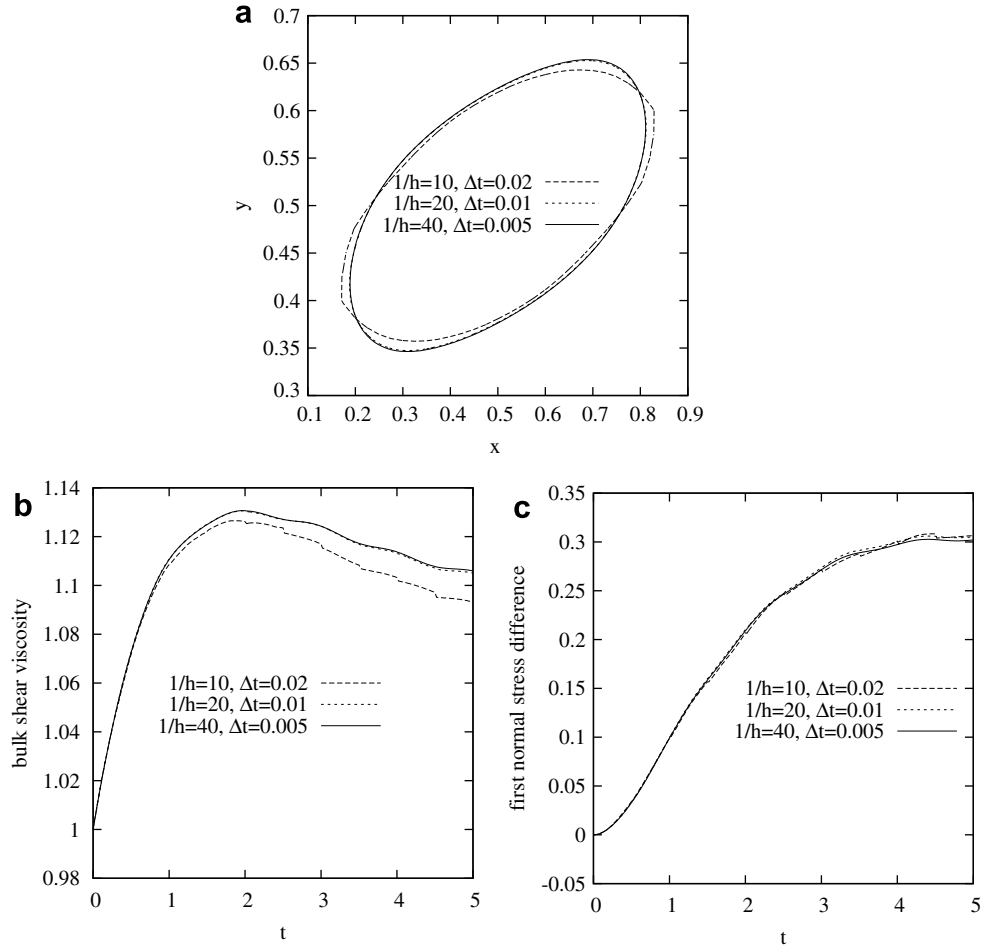

Fig. 3. The mesh refinement results from the single drop of radius 0.2 initially at the domain center: (a) the deformed shape of the drop at $t = 4.8$; (b) the bulk shear viscosity; (c) the bulk first normal stress difference.

Table 1
The mesh refinement result for the single drop of radius 0.2 initially located at the domain center (Fig. 3)

Mesh	Δt	Error in the shear viscosity	Error in first normal stress difference
10×10	0.02	6.04867×10^{-3}	2.10774×10^{-3}
20×20	0.01	2.79408×10^{-4}	1.68454×10^{-3}
40×40	0.005	(–)	(–)

Considering the case of $h = 1/40$ with $\Delta t = 0.005$ as the reference data, the 1-norm error of the bulk stress has been presented for the data in time.

difference. The necessity of sub-division is obvious, as expected from the interpretation in Fig. 2 in Section 3.2. Without the sub-division of the element (1×1), the calculated drop size is found to be smaller than it should be and the bulk stress also shows large discrepancy compared with that of other cases. From Fig. 4, one may conclude that the 4×4 is an optimal choice considering both the computational cost and the accuracy. This result can be anticipated: the line segments in the 1×1 and 2×2 sub-divisions cannot utilize the full geometrical information from the discontinuous quadratic interpolation that has been used for ϕ.

5.1.3. The split drop

Next, we compare the result of the single drop initially located at the center of the domain $(0.5, 0.5)$ and that initially located at the corner of the domain $(0, 0)$. In the latter case, the drop is split into four parts initially. By

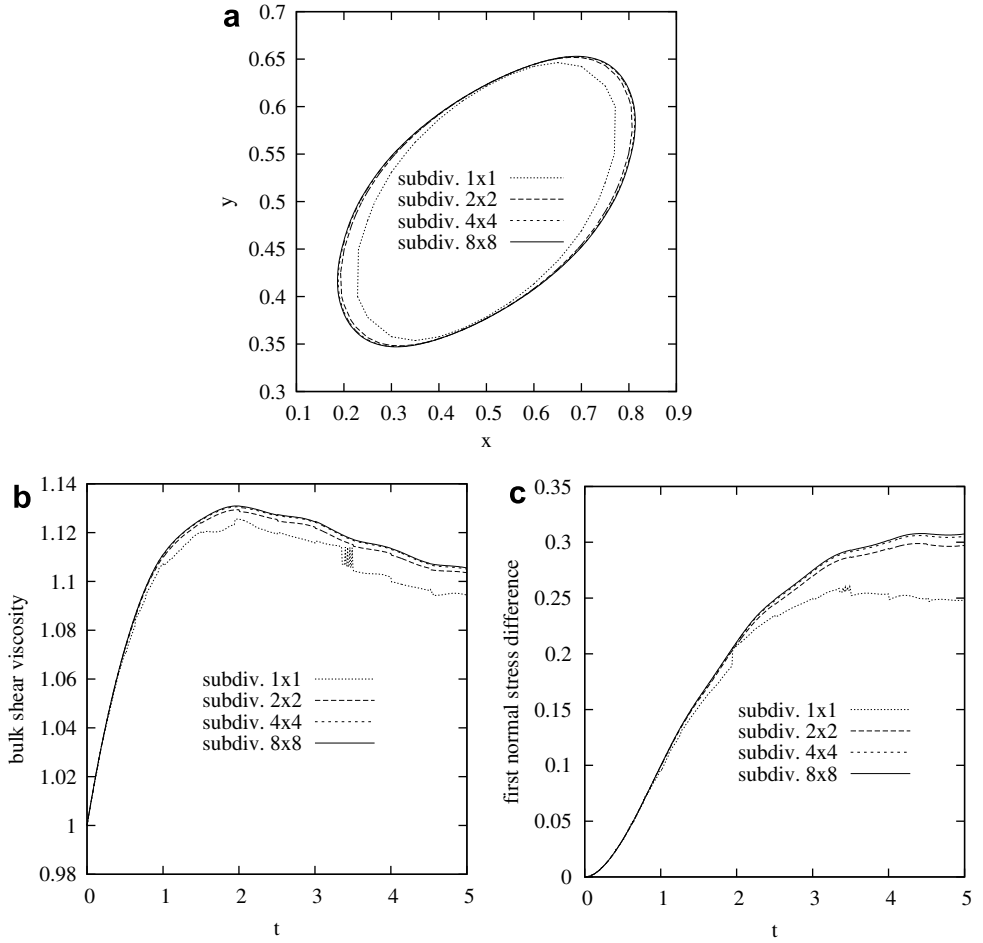

Fig. 4. The effect of the degree of sub-division of the element in finding the line segments along the interface using the single drop of radius 0.2 initially at the domain center: (a) the deformed shape of the drop at $t = 4.8$; (b) the bulk shear viscosity; (c) the bulk first normal stress difference.

Table 2
The effects of the degree of sub-division of the element in finding line segments along the interface using the single drop of radius 0.2 initially located at the center (Fig. 4)

Number of sub-division	Error in the shear viscosity	Error in first normal stress difference
1×1	7.63792×10^{-3}	2.35970×10^{-2}
2×2	1.78866×10^{-3}	4.24901×10^{-3}
4×4	3.23887×10^{-4}	9.39442×10^{-4}
8×8	(–)	(–)

The fixed mesh $h = 1/20$ and the time step $\Delta t = 0.01$ have been used for comparison and, considering the 8×8 subdivision data as the reference data, the 1-norm error of the bulk stress has been presented for the data in time.

definition of the sliding bi-periodic frame, the two problems should show identical solutions for the deformation shape and the quantities of the bulk shear stress and the first normal stress difference. This is quite an important test in this work, since there should not be any restriction on the droplet configuration, i.e., droplets should be able to cross any part of the computation domain boundary freely. In this way, the complicated wall interaction can be avoided and then the sliding frame plays the role of a representative "window" for flowing materials.

Considering the results from the drop initially located at the center with $h = 1/40$ and $\Delta t = 0.005$ as the reference, we presented the mesh refinement results of the drop initially located at the corner for the drop deformation shape at $t = 4.8$ and the bulk stress responses in Fig. 5 and in Table 3. For the corner drop case, we use again the fluid meshes of 10×10 (denoted by $h = 1/10$), 20×20 ($h = 1/20$) and 40×40 ($h = 1/40$) and the corresponding time steps Δt are 0.02, 0.01 and 0.005, respectively. We use the 4×4 sub-division of elements for all these simulations. Note that, for $t = 4.8$, the upper (and thereby lower) drop interfacial segments travel more than two turns on the sliding boundary. In Fig. 5(a), we translated the deformed shape of the drop initially located at the center to overlap the results from the corner drop for a proper comparison. The results of the deformed shape and the bulk shear viscosity for the split drop show excellent mesh convergence to the reference one. There can be observed a small discrepancy in the first normal stress difference (Table 3). Again, for the drop radius 0.2 initially located at the corner, the $h = 1/10$ mesh has been found not to be enough to predict the drop deformation shape as well as the bulk shear viscosity.

5.1.4. Computation of the bulk stress

The final verification is about the computation of the bulk stress. In Section 4, we mentioned that there are two methods in evaluating the bulk stress: one is the boundary integral using the Lagrangian multipliers

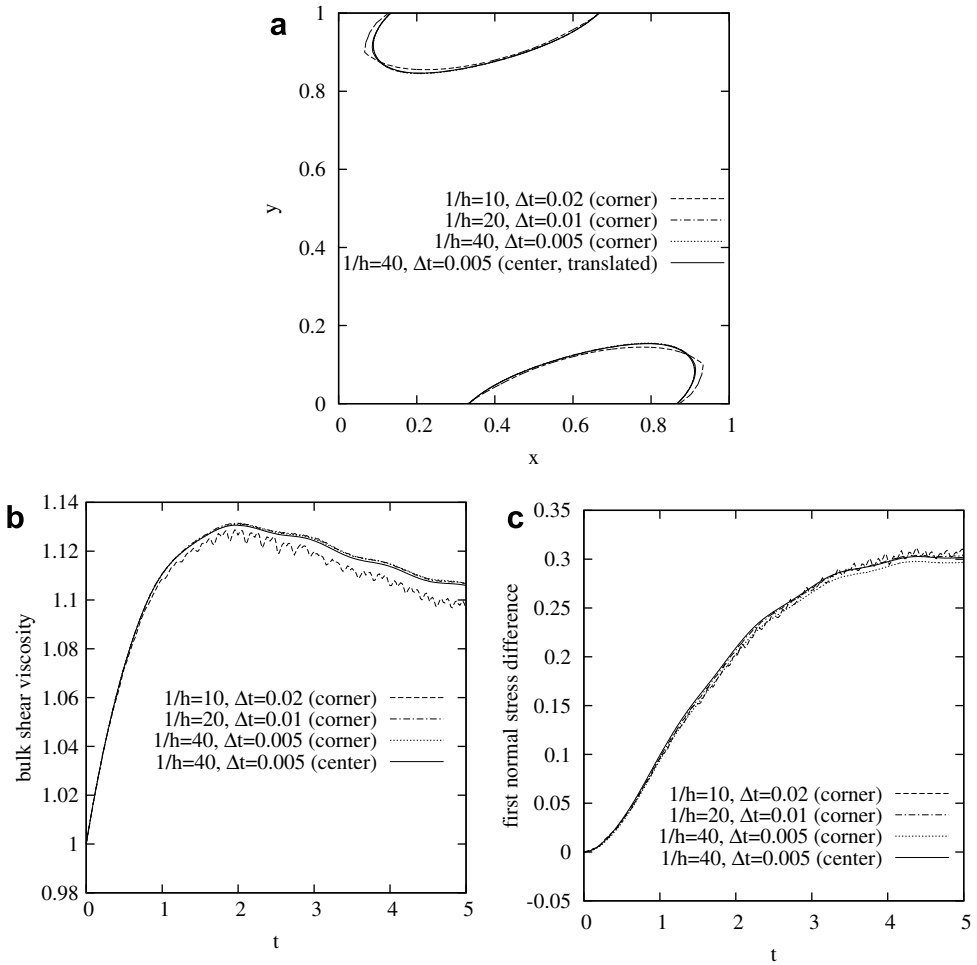

Fig. 5. The comparison of the results of the single drop $R = 0.2$ initially at the center of domain $(0.5, 0.5)$ with those at the corner of the domain $(0, 0)$: (a) the deformed shape of the drop at $t = 4.8$; (b) the bulk shear viscosity; (c) the bulk first normal stress difference. The deformed shape of the drop initially at the domain center has been translated to the boundary for better comparison in (a).

Table 3
The comparison of the bulk stress results of the single drop of radius 0.2 initially at the domain center and the corner of the domain (Fig. 5)

Mesh	Δt	Error in the shear viscosity	Error in first normal stress difference
10×10 (corner)	0.02	4.17208×10^{-3}	3.86897×10^{-3}
20×20 (corner)	0.01	6.58910×10^{-4}	1.44879×10^{-3}
40×40 (corner)	0.005	5.51008×10^{-4}	5.07814×10^{-3}
40×40 (center)	0.005	(–)	(–)

Considering the case of $h = 1/40$ with $\Delta t = 0.005$ when the drop located at the domain center as the reference data, the 1-norm error of the bulk stress for the drop initially at the corner has been presented for the data in time.

(Eqs. (35)) and the other is the domain integral using the continuous surface stress $\boldsymbol{\tau}^s$ from the CSS formulation (Eqs. (33) and (36)). We use the $h = 1/20$ mesh with $\Delta t = 0.01$ and the 4×4 sub-division of the element for the single drop at the center of the domain. The bulk shear viscosities and the first normal stress difference from the two different methods are presented in Fig. 6. The two results coincide exactly with each other which verifies the proper implementation of the sliding bi-periodic boundary condition and the bulk stress evaluation in the bi-periodic matrix/drop mixture system.

5.2. Coalescence of two drops in a sliding bi-periodic frame

The second example problem is constructed to investigate the effect of hydrodynamic and interfacial interaction between two drops, especially, the coalescence of the two drops. Also we are interested in the bulk stress response during the coalescence process. The coalescence relies on an agent to push drops together (e.g. body force, external flow), as well as short-range molecular force (e.g. van der Waals attraction) that rupture the thin liquid film that separates drop interfaces prior to confluence [29]. If the van der Waals force is not considered, the drop coalescence will be the numerical artifact due to the course mesh in between droplets in the interface-capturing method like the level-set method used here [30,31]. Nevertheless, in this study, results are presented for drop coalescence as the same way as done in Ref. [9] with neglecting the van der Waals forces between two droplets in order to see the possibilities of coalescence and typical flow fields before and after coalescence together with resultant bulk stress responses.

The problem is stated as follows: two identical drops of radius $R = 0.2$ are suspended freely in a sliding bi-periodic frame of the size 1×1. The viscosity of the drop is the same as that of the matrix and the surface tension ζ is 5 and the applied shear rate $\dot{\gamma}$ is 1. The capillary number Ca is 0.1. The initial drop positions are chosen symmetrically: $(0.35, 0.65)$ and $(0.65, 0.35)$. Since the reference velocity has been specified zero at

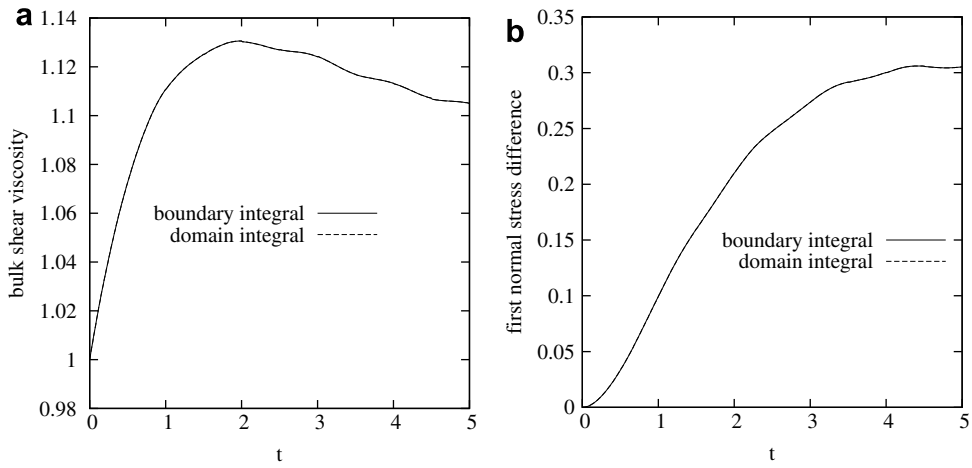

Fig. 6. The comparison of (a) the bulk shear viscosity and (b) the first normal stress by two different calculation techniques: the domain integral method based on the CSS formulation (Eqs. (33) and (36)) and the boundary integral method in Eqs. (35).

the center of the left domain boundary (Γ_4), the upper left drop is supposed to move to the positive x direction and the lower right one to the negative x direction. We tested two different meshes of $h = 1/20$ and $h = 1/50$ and the corresponding time steps Δt are 0.005 and 0.001, respectively.

Fig. 7 shows the computed drop shapes at every $t = 0.1$ time elapse from $t = 0$ using the two meshes. The drop shape is represented by the line segments satifying $\phi = 0$ along the interface. The oscillation in the coarse mesh result at $t = 0$ is caused by the fact that the distance between the two drop interfaces is too small compared with the size of the element. The coalescence has been finished within $t = 0.3$ and then the merged drop becomes circular again. (As mentioned, this coalescence is a numerical artifact and is an inherent limitation of the interface capturing method like the level-set method used here.) The phenomena observed from the two meshes are mostly identical. We see some discrepancy of the coarse mesh problem during the fast coalescence in the early period. Plotted in Fig. 8 are the bulk shear viscosity and the first normal stress difference evaluated during this coalescence process. We presented the bulk responses for both coarse and fine meshes for comparison. The basic trend are the same: during fast coalescence, the shear viscosity and the first normal stress difference decrease fast and then they recover the values for the large single merged drop. Though the behavior is nearly identical, there can be observed a small discrepancy in the result of the coarse mesh especially in the early period.

One interesting phenomena is the negative value of the shear viscosity and the first normal stress difference during the early phase of the coalescence. The negative value of the shear viscosity indicates that the shear stress developed by the interfacial-tension-driven flow, opposed to the direction of the given shear flow, dominates over the shear stress due to the assigned shear rate in the early period of the coalescence. The interfacial-tension-driven flow is spontaneous and it lowers the level of the shear stress, until the single merged drop restores the circular shape. As the single merged drop stretches due to the shear flow, the behavior of the shear viscosity becomes similar to that of the single particle problem presented in Section 5.1. The negative first normal stress in the system implies that the coalescence generates a squeezing force. Imagine a simple shear flow confined two parallel plates that contain the droplet emulsions. Then the upper plate tends to be pushed down due to this negative first normal stress during the coalescence of relatively large drops. The first normal stress difference is restored positive, as in the single drop problem, when the single merged drop starts to stretch in the flow direction. This interpretation can be understood by looking at the instantaneous velocity field at $t = 0.2$ (near the minimum of the shear viscosity and the first normal stress difference) presented in Fig. 9.

5.3. The multiple droplet problem

Now we proceed to a more complex problem: six randomly distributed drops in the sliding bi-periodic frame initially. The main objective here is to demonstrate the feasibility of the present work for the application

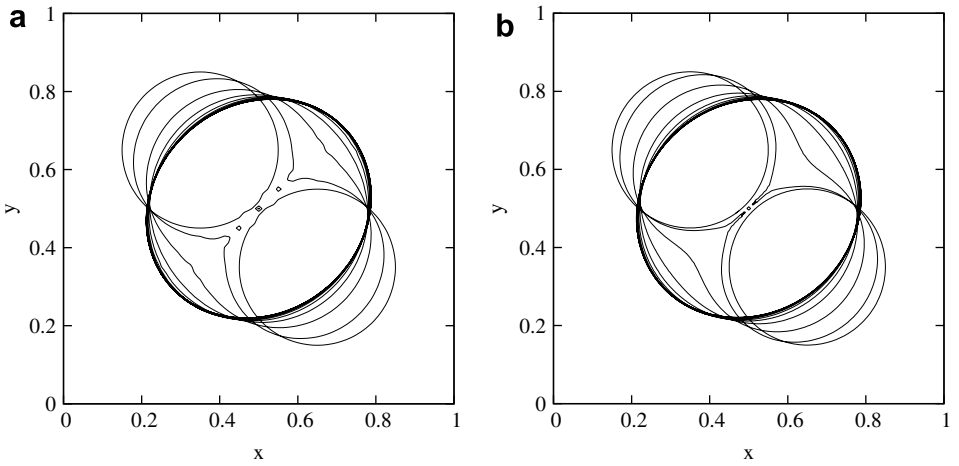

Fig. 7. The coalescence of the two drops: (a) with the $h = 1/20$ mesh and (b) with the $h = 1/50$ mesh. The computed drop shapes are represented by the line segments along the interface at every $t = 0.1$ time elapse.

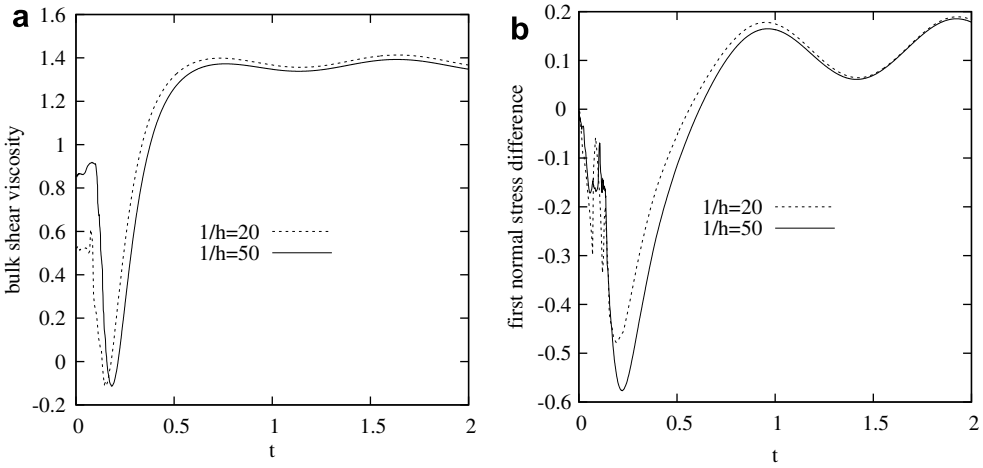

Fig. 8. The comparison of the bulk rheological behavior computed using the coarse (20×20) and fine (50×50) meshes: (a) the bulk shear viscosity and (b) the first normal stress difference.

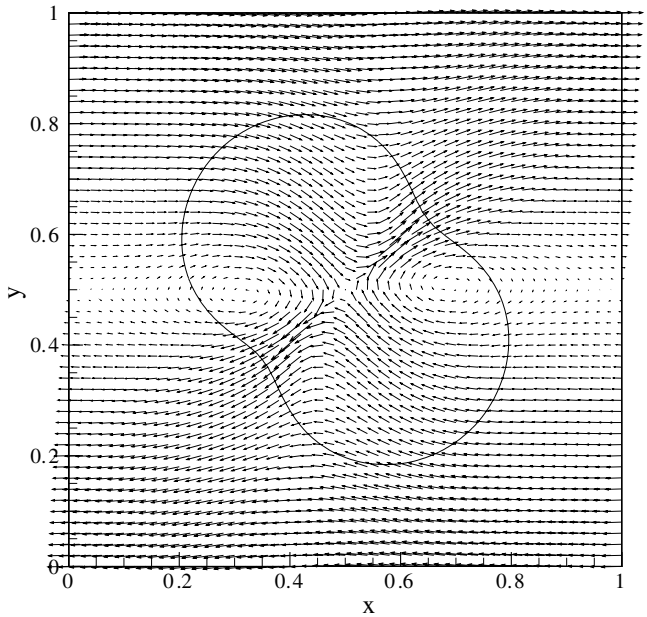

Fig. 9. The velocity field during the coalescence of the two drops ($t = 0.2$ using $h = 1/50$ mesh).

to rheology of concentrated droplet emulsions with complicated drop/fluid and drop/drop interactions and with the interfacial tension. The problem is stated as follows: we initially placed six randomly distributed circular drops with different radii, $R = 0.075$, 0.1 (two drops), 0.125, 0.15 and 0.175, in a sliding bi-periodic frame of size 1×1. The viscosity of the drop is the same as the matrix fluid and the surface tension ζ is given 0.05. We use a $h = 1/50$ mesh with the time step $\Delta t = 0.005$. The problem is composed of two step procedures: first, we applied the simple shear with the shear rate $\dot{\gamma} = 1$ for $t = 6$ and then we stopped the flow to investigate the relaxation phenomena.

Presented in Fig. 10 are the morphological evolution of the droplet deformation followed by the relaxation. As mentioned, the droplets elongate until $t = 6$ due to the shear flow and then they start to relax. Even at $t = 40$, the relaxation is still present especially for large drops. In Fig. 11, we plotted the distribution of the distance function d and the 11-component of the interfacial stress $\boldsymbol{\tau}_s$ over the domain at the final time step

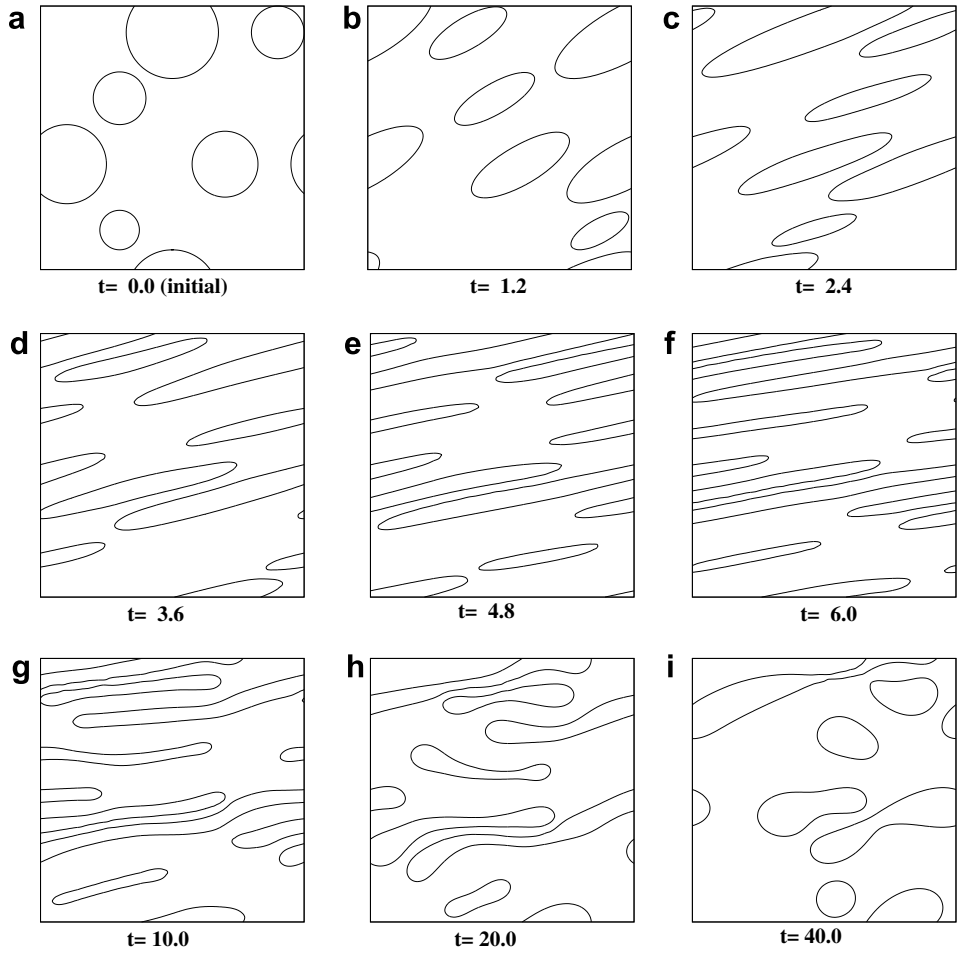

Fig. 10. The morphological evolution of six randomly distributed drops under the start-up of simple shear flow followed by the relaxation. The shear flow was stopped at $t = 6$.

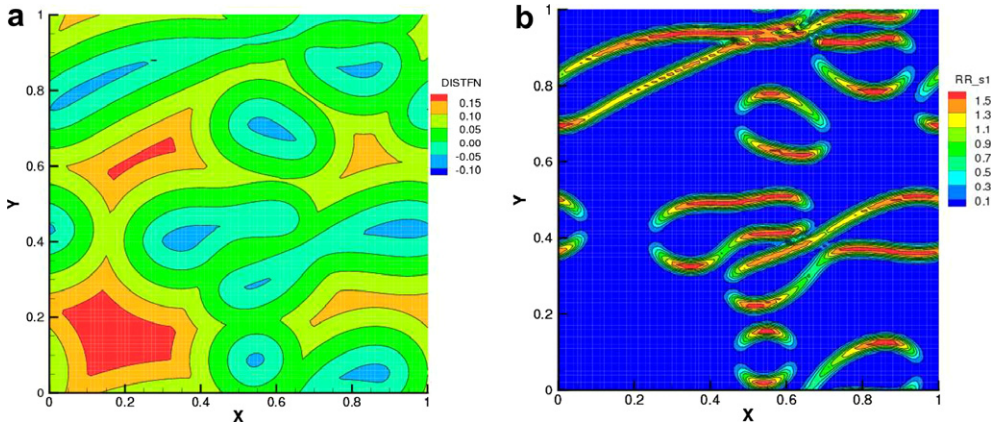

Fig. 11. The distributions of (a) the distance function d and (b) the 11-component of the continuous surface stress τ_s for the final droplet configuration in the multiple droplet example problem ($t = 40.0$).

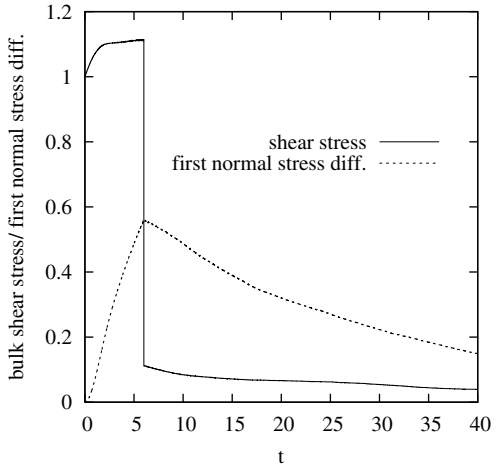

Fig. 12. The bulk shear stress and the first normal stress difference in the multiple droplet example problem.

$t = 40$. One can compare the drop deformation pattern in Fig. 10(i) with these results. As shown in Fig. 11(a), one can see that the signed distance function property is well satisfied with this concentrated droplet emulsion problem in the sliding bi-periodic frame. Also the continuous surface stress distribution along the periodic boundary and on the interface of the droplet indicates the appropriateness of our formulation/implementation.

Finally, we presented the bulk shear stress $\langle\sigma_{12}\rangle$ and the first normal stress difference with respect to time in Fig. 12. Both stresses increase as droplets elongate until $t = 6$ and then sudden decrease has been observed in both stress results. After the cessation of the flow during relaxation, the interfacial contribution constitutes a major contribution to the bulk stress, as expected from Eq. (33). This interfacial contribution will eventually vanish as droplets becomes circular as well. The bulk stresses in Fig. 12 show such a relaxation process. A similar experiment was performed by Cristini et al. [32] to investigate the transient stress behavior under the start-up of shear flow followed by the relaxation at a certain time. Though not directly comparable (the experiment is 3D), their experimental data shows much stiffer decrease of the shear stress after stopping the flow than the first normal stress difference, which is identical to the result in Fig. 12 in the present work.

6. Conclusions

In this work, we developed a direct numerical simulation technique for the droplet emulsion in the sliding bi-periodic frame, which is quite well suited for studying rheology and micro-structural morphological developments of such a system in simple shear flow. In our formulation, the level-set method with the continuous surface stress formulation has been combined, for description of the interfacial tension, with the sliding bi-periodic frame based on the finite-element method. The present scheme can be extended relatively easily to the viscoelastic liquid–liquid emulsion which is of great importance in polymer industry. We use a direct geometrical re-distancing method to obtain the signed distance function using line segments along the interface that satisfies the sliding bi-periodicity of the computational domain. The line segment representing the interface has been searched on the sub-divided element boundary. We use the mortar element technique for implementation of the sliding periodicity. The third-order non-oscillating TVD-RK3 time-stepping method has been combined with the discontinuous Galerkin method in solving the advection equation of the level-set function. In our formulation the bulk stress can be evaluated by the line integral of the Lagrangian multipliers used for the periodicity constraint.

Concentrating on 2D droplet emulsion problems, we tested numerical examples of the single, two and multiple drops in a sliding bi-periodic frame, representing a large number of repeated structures, for the verification of the code and also for the presentation of the feasibility of our scheme. In the single drop problem, we proved the mesh refinement of our solution and investigated the effect of the number of sub-division of the

element on the solution, when finding line segments along the interface. We also verified the accuracy and convergence of the solution for the split drop, which crosses the computational domain boundary. This is a quite important test in the bi-periodic simulation of a representative unit cell problem. The comparison of the bulk stresses, evaluated by the domain integral of equi-viscous system with the CSS formulation and the boundary integral of the Lagrangian multipliers, verifies the proper implementation of the sliding bi-periodic boundary condition and the bulk stress evaluation in the bi-periodic matrix/drop mixture system.

Using two droplets in a sliding bi-periodic frame, we demonstrated the feasibility of capturing the morphological development during the coalescence process in the absence of the short-range van der Waals force. During the coalescence, an instantaneous decrease of the shear viscosity and the first normal stress difference has been observed due to the compressive flow in the direction opposed to the given shear flow generated by the coalescence. Finally in the multiple droplet problem, we investigated the deformation and the relaxation of droplets by the cessation of the flow followed by simple shear flow for a certain period, as a model droplet emulsion problem.

Acknowledgments

This work has been supported by the Basic Research Program of the Korea Science and Engineering Foundation (Grant No. R01-2006-000-10267-0 for W.R.H. and R02-2001-000-01215-0 for S.J.K.) and the Korea Research Foundation Grant (KRF-2005-005-J09902) by the Korean government (MOEHRD). The authors also acknowledge fruitful discussions with Dr. Tae Gon Kang in implementing the TVD-RK3 scheme.

References

[1] C.D. Han, Multiphase flow in polymer processing, Academic, New York, 1981.
[2] C.L. Tucker, P. Moldenaers, Microstructural evolution in polymer blends, Ann. Rev. Fluid Mech. 34 (2002) 177.
[3] A.W. Lees, S.F. Edwards, The computer study of transport processes under extreme conditions, J. Phys. C: Solid State Phys. 5 (1972) 1921.
[4] A.J. Wagner, I. Pagonabarraga, Lees–Edwards boundary conditions for Lattice Boltzmann, J. Statist. Phys. 107 (2002) 521.
[5] A. Lamura, G. Gonnella, Lattice Boltzmann simulations of segregating binary fluid mixtures in shear flow, Physica A (2001) 295.
[6] X.F. Yuan, M. Doi, A general approach for modelling complex fluids: its application to concentrated emulsions under shear, Colloids Surf. A: Physicochem. Eng. Aspects 144 (1998) 305.
[7] W.R. Hwang, M.A. Hulsen, H.E.H. Meijer, Direct simulation of particle suspensions in sliding bi-periodic frames, J. Comput. Phys. 194 (2004) 742.
[8] W.R. Hwang, M.A. Hulsen, H.E.H. Meijer, Direct simulations of particle suspensions in a viscoelastic fluid in sliding bi-periodic frames, J. Non-Newtonian Fluid Mech. 121 (2004) 15.
[9] P.D. Anderson, B.J. Keestra, M.A. Hulsen, On the streamline-vorticity formulation in sliding bi-periodic frames: application to bulk behavior for polymer blends, J. Comput. Phys. 212 (2005) 268.
[10] F.P.T. Baaijens, Mixed finite element method for viscoelastic flow analysis: a review, J. Non-Newtonian Fluid Mech. 79 (1998) 361.
[11] V. Cristini, J. Blawzdziewicz, M. Loewenberg, Drop breakup in three-dimensional viscous flows, Phys. Fluids 10 (1998) 1781.
[12] S.J. Kim, C.D. Han, Finite element analysis of axisymmetric creeping motion of a deformable non-Newtonian drop in the entrance region of a cylindrical tube, J. Rheol. 45 (2001) 1279.
[13] S.J. Kim, S.D. Kim, Y. Kwon, Deformation of multiple non-Newtonain drops in the entrance region, Korea–Australia Rheol. J. 15 (2003) 75.
[14] S. Ramaswamy, L.G. Leal, The deformation of a Newtonian drop in the uniaxial extensional flow of a viscoelastic liquid, J. Non-Newtonian Fluid Mech. 88 (1999) 149.
[15] J. Li, Y. Renardy, Shear-induced rupturing of a viscous drop in a Bingham liquid, J. Non-Newtonian Fluid Mech. 95 (2000) 235.
[16] S. Osher, J. Sethian, Front propagating with curvature dependent speed: algorithm based on Hamilton–Jacobi formulations, J. Comput. Phys. 79 (1998) 12.
[17] S. Osher, S. Fedkiw, Level set methods and dynamics implicit interfaces, Springer-Verlag, New York, 2003.
[18] Y.C. Chang, T.Y. Hou, B. Merriman, S. Osher, A level-set formulation of Eulerian interface capturing methods for incompressible fluid flows, J. Comput. Phys. 124 (1996) 449.
[19] P. Yue, J.J. Feng, C. Liu, J. Shen, A diffuse–interface method for simulating two-phase flows of complex fluids, J. Fluid Mech. 515 (2004) 293.
[20] J.U. Brackbill, D.B. Kothe, C. Zemach, A continuum method for modeling surface tension, J. Comput. Phys. 100 (1992) 335.
[21] B. Lafaurie, C. Nardone, R. Scardovelli, S. Zaleski, G. Zanetti, Modelling merging and fragmentation in multiphase flow with SURFER, J. Comput. Phys. 113 (1994) 134.
[22] M. Fortin, A. Fortin, A new approach for the FEM simulation of viscoelastic flows, J. Non-Newtonian Fluid Mech. 32 (1989) 295–310.

[23] Y.R. Tsai, Rapid and accurate computation of the distance function using grids, J. Comput. Phys. 178 (2002) 175.
[24] C.W. Shu, S. Osher, Efficient implementation of essentially non-oscillatory shock capturing scheme, J. Comput. Phys. 77 (1988) 439.
[25] P.R. Amestoy, I.S. Duff, Vectorization of a multiprocessor multifrontal code, Int. J. Supercomput. Appl. 3 (1989) 41.
[26] P.R. Amestoy, I.S. Duff, Memory management issues in sparse multifrontal methods on multiprocessors, Int. J. Supercomput. Appl. 7 (1989) 64.
[27] P.R. Amestoy, C. Puglisi, An unsymmetrized multifrontal LU factorization, SIAM J. Matrix Anal. Appl. 24 (2002) 553.
[28] T. Jansseune, I. Vinckier, P. Moldenaers, J. Mewis, Transient stresses in immiscible model polymer blends during start-up flows, J. Non-Newtonian Fluid Mech. 99 (2001) 167.
[29] M.B. Nemer, X. Chen, D.H. Papadopoulos, J. Blawzdziewicz, M. Loewenberg, Hindered and enhanced coalescence of drops in Stokes flows, Phys. Rev. Lett. 92 (2004) 114501.
[30] P. Yue, J.J. Feng, C. Liu, J. Shen, Diffuse-interface simulations of drop coalescence and retraction in viscoelastic fluids, J. Non-Newtonian Fluid Mech. 129 (2005) 163.
[31] P.J.A. Janssen, P.D. Anderson, G.W.M. Peters, H.E.H. Meijer, Axisymmetric boundary integral simulations of film drainage between two viscous drops, J. Fluid Mech. 567 (2006) 66.
[32] V. Cristini, C.W. Macosko, T. Jansseune, A note on transient stress calculation via numerical simulations, J. Non-Newtonian Fluid Mech. 105 (2002) 177.